Received: 21 October 2020 | Revised: 9 December 2020 | Accepted: 26 December 2020

DOI: 10.1002/poc.4188

RESEARCH ARTICLE

Journal of Physical Organic Chemistry WILEY

# Experimental and theoretical studies of 1,3,5-tris (bromomethyl)-2,4,6-trimethylbenzene with 2-pyridone

**R. Nandini Asha**[1,2] | **M. Usha Rahini**[1,2] | **Caroline Daisy**[1,2] | **B. Ravindran Durai Nayagam**[1,2] | **N. Bhuvanesh**[3]

[1]Department of Chemistry and Research Centre, Popes' College (Autonomous), Sawyerpuram, Tuticorin, 628251, India

[2]Manonmaniam Sundaranar University, Tirunelveli, India

[3]Department of Chemistry, Texas A&M University, College Station, TX, USA

**Correspondence**
B. Ravindran Durai Nayagam, Department of Chemistry and Research Centre, Popes' College (Autonomous), Sawyerpuram-628251, Affiliated to Manonmaniam Sundaranar University, Tirunelveli-627012, Tamil Nadu, Tuticorin, India.
Email: b_ravidurai@yahoo.com

**Abstract**

In this present work, a new compound 1-({2,4,6-trimethyl-3,5-bis[(2-oxo-2H-pyridin-1-yl)methyl]phenyl}methyl)-2H-pyridin-2-one hydrate (M3P) has been synthesized and characterized by IR, $^{1}H$, and $^{13}C$ NMR and single-crystal X-ray diffraction analysis. The molecular geometry, frontier molecular orbital energies, and thermodynamic properties of the title molecule were explored using density functional theory (DFT) calculation via B3LYP method with 631 ++G (d,p) basis set. The compound (M3P) crystallizes in the space group of P-1 with unit cell parameter a = 9.8224(12) Å, b = 11.6383(14) Å, c = 11.8865 (14) Å, α = 64.6410(10)°, β = 81.156(2)°, γ = 69.5910(10)°, V = 1150.8(2) Å3, and Z = 2. Furthermore, Hirshfeld surface analysis was performed to observe better intermolecular interactions in the crystal packing. The nature of the interaction of M3P with DNA and BSA protein was studied using molecular docking analysis. DNA binding studies were also done using UV spectrophotometric method. The compound moderately binds with CT-DNA which is comparable with the docking results. in vitro anti-microbial activities against some bacterial and fungal strains were investigated. M3P shows good response against bacteria *Pseudomonas aeruginosa* and *Klebsiella pneumonia* and fungi *Candida albicans* and *Aspergillus niger*.

**KEYWORDS**

2-pyridone, DFT, DNA binding, Hirshfeld surface analysis, molecular docking

## 1 | INTRODUCTION

Heterocyclic compounds are one of the important categories of organic compounds. A huge number of organic compounds used in the medicinal field as drugs for various diseases contain heterocyclic skeletons inclusive of antibacterial, antifungal, antioxidants, and anticancer, and so on.[1] Pyridones are a unique class of six-membered aza-heterocycles and are present in several natural and biologically active scaffolds.[2,3] Many researchers have shown great interest in the synthesis of pyridone chemistry due to their vast biological applications. The 2-pyridone compounds display numerous pharmacological activities like antibacterial,[4] antifungal,[5] anti-inflammatory,[6] antiviral,[7] antitumor,[8] and anti-Alzheimer's properties.[9] Due to a peptidomimetic functionality of 1H-pyridin-2-one tautomer, it plays an essential role as a scaffold in drug design.[10,11] The 2-pyridone core and its tautomer, 2-hydroxypyridine, have been reported as a feature of several new NSAIDs.[12–14] In recent years, 2-pyridones have captivated much importance as these compounds have been found to exhibit several biological activities, such as

  

HIV-1 non-nucleoside reverse transcriptase inhibitors (NNRTIs) and cardiotonic agents.[15,16] Amrinone is a therapeutic drug candidate containing pyridine structural unit which is used in the treatment of heart failure diseases.[17] 1H-pyridin-2-ones are also promising compounds for the preparation of modified nucleotides and oligonucleotides.[18–21] The 2-pyridone skeleton with the cis-amide substructure provides an ideal structure for bifunctional catalysis and also supramolecular structures.

Moreover, 2-pyridones are of particular interest to researchers due to their in vitro and in vivo antibacterial potencies against the bacterial type II DNA topoisomerases, which includes two highly homologous enzymes DNA gyrase and topoisomerase IV.[22] A series of novel compounds like 6-amino-1-((1,3-diphenyl-1H-pyrazole-4-yl)methyleneamino)-4-(aryl)-2-oxo-1,2-dihydropyridine-3,5 dicarbonitriles were synthesized and screened for their in vitro antibacterial activity against *Staphylococcus aureus*, *Streptococcus pyogenes* (Gram positive), *Escherichia coli*, *Pseudomonas aeruginosa* (Gram negative) by broth dilution and cytotoxic activity by MTT assay. Pyridone derivatives have been used as enzymes inhibitors.[23,24] The results indicated that the compounds exhibited potent antibacterial activity against bacterial strains at non-cytotoxic concentrations.[25] A 2-pyridone derivative namely perchlorate salt of 1-(2-aminoethyl)-6-hydroxy-2-oxo-4-(3-pyridinyl)-1,-2-dihydropyridine-3,5-dicarbonitrile was synthesized by a group of researchers, and its interaction with CT-DNA was explored. It was observed that the compound can bind to the DNA helix in a partial intercalative manner.[26]

Density functional theory (DFT) calculations in conjugation with molecular docking analysis are inevitable in exposing the nature of interactions between compounds and protein in recent years.[27,28] It is important to note that various forces including hydrogen bonding, π– π stacking, and electrostatic interactions along with other non-covalent interactions help the molecules to be intact inside the binding pocket of proteins. Geometry optimization of compounds using DFT calculations followed by frontier molecular orbital analysis can be done to understand the nature of binding of these compounds into the BSA from molecular docking analysis.

In view of the above facts, we have synthesized a novel 2-pyridone derivative M3P from 1,3,5-tris (bromomethyl)-2,4,6-trimethylbenzene and sodium salt of 2-pyridone. The synthesized compound has been confirmed by spectroscopic reports. Furthermore, DFT calculations, Hirshfield surface analysis, biological studies like docking with DNA and BSA protein, antimicrobial activities, and DNA binding studies of the newly prepared compound have been investigated.

## 2 | EXPERIMENTAL METHODS

### 2.1 | General methods

All chemicals and solvents were acquired from commercial sources with high purity and analar grade and used as received unless otherwise noted. The melting point of the title compound was measured in an open capillary tube. The infrared spectrum was recorded on a JASCO 4600 (Japan) FT-IR spectrometer (in KBr pellet) with a scan range from 400 to 4,000 $cm^{-1}$. $^{1}H$- and $^{13}C$-NMR spectra were recorded with a Bruker Avance III, 400 MHz, 9.4 Tesla superconducting magnet using $CDCl_3$ as a solvent. Chemical shifts were reported as δ (ppm) with tetramethylsilane as an internal standard. DNA binding experiments were done using Jasco V-650 UV spectrophotometer.

### 2.2 | Synthesis of 1,3,5-tris (bromomethyl)-2,4,6-trimethylbenzene

Mesitylene (12.0 g, 0.100 mol), paraformaldehyde (10.0 g, 0.330 mol), and 50 ml of glacial acetic acid were mixed with 70 ml of 31% HBr/acetic acid solution. The mixture was kept for 12 h at 120°C and then poured into 100 ml of water. The product 1,3,5-tris (bromomethyl)-2,-4,6-trimethylbenzene was filtered and dried in vacuum at room temperature.[29]

### 2.3 | Synthesis of ({2,4,6-trimethyl-3,5-bis [(2-oxo-2H-pyridin-1-yl)methyl]phenyl} methyl)-2H-pyridin-2-one hydrate (M3P)

A mixture of 2,4,6-tris (bromomethyl)mesitylene (0.399 g, 0.001 mol) and 2-hydroxypyridine sodium salt (0.285 g, 0.003 mol) in water (30 ml) and methanol (30 ml) was heated at 80°C with stirring for 60 min. The compound formed was filtered and dried (Scheme 1). It was then dissolved in chloroform and methanol (1:2 v/v) and allowed to undergo slow evaporation process for a week. Fine crystals were obtained. The purity of the compound was checked by performing TLC, and the yield was noted as 85%. M.Pt°C: 263.6. **FT-IR (KBr, $cm^{-1}$)**: 3731.58, 2920.16, 2361.41, 1735.62, 1665.59, 1598.7, 1472.38, 1377.89, 1235.18, 1019.19, 1022.09, 991.232, 867.81, 648.929, 509.115, 409.709 ( Figure S1). **$^{1}H$ NMR ($CDCl_3$)**

**SCHEME 1** Synthesis of M3P

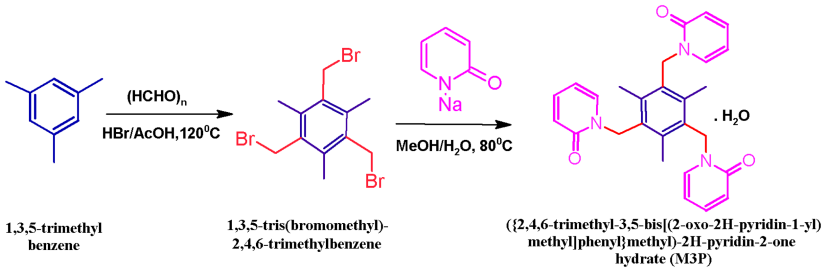


**δ ppm:** Py-H 7.33 (t, 1H), 6.74 (d, 1H), 6.65(d, 1H), 6.10 (t, 1H), N-$CH_2$-5.22 (s,2H) and -$CH_3$ 2.21 (s,3H) (Figure S2). **$^{13}$C NMR (300 MHz $CDCl_3$) δ ppm**: 15.26, 44.99, 105.25, 119.40, 130.16, 132.16, 138.04, 139.40,161.60(C=O) (Figure S3).

## 2.4 | X-ray structure determination

Single crystals obtained were characterized using a BRUKER Quest X-ray (fixed-Chi geometry) diffractometer. The goniometer was controlled using the APEX3 software suite.[30] The absorption correction program SADABS[31] was employed to correct the data for absorption effects. Systematic reflection conditions and statistical tests of the data suggested that the space group P-1. A solution was obtained readily using XT/XS in APEX3. The absence of additional symmetry and voids was confirmed using PLATON (ADDSYM). The structure was refined (weighted least squares refinement on $F^2$) to convergence.[32–35] Olex 2 was employed for the final data presentation and structure plots.[36] Mercury 3.0 was used for generating structures and molecular interaction drawings.

## 2.5 | Hirshfeld surface analysis

Intermolecular interactions, as well as surface properties of the pro-molecule of **M3P**, were defined by Hirshfeld surface[37] and 2D fingerprint plots[38] which were successfully acquired from CrystalExplorer-17.5[39] using the cif files of SCXRD data.

## 2.6 | Computational methodology

The single-crystal structure file (cif file) of the title compounds was converted to mol2 files using Mercury 3.0. These files were used as input files in the GAMESS (US) software package[40] for energy and other calculations. Theoretical calculation of **M3P** in the gas phase was performed using the analytical gradient method of DFT with Becke's three parameters (B3) exchange functional together with the Lee-Yang-Parr (LYP) non-local correlation functional, symbolized B3LYP using 6-311G++ basis set. Parameters such as ionization potential (I), electron affinity (A), electronegativity (χ), electrochemical potential (μ), hardness (η), softness (σ), and electrophilicity index (ω) were calculated using previous reports.[41–43]

## 2.7 | Molecular docking studies

Molecular docking analysis was performed using Auto Dock Vina software where an optimized structure of **M3P** has been used.[44] DNA docking analysis of **M3P** has been done by using the crystal structure of DNA duplex of sequence d (CGCGAATTCGCG)2 dodecamer (PDB ID:1BNA). Molecular docking studies have also been carried out using BSA protein structure (PDB ID: 4F5S) which was downloaded from a protein data bank (PDB).[45] The interactions of M3P with DNA/BSA, including hydrogen bonds and hydrophobic interactions, were analyzed using Discovery studio 4.0 client[46] and PyMol.[47]

## 2.8 | Antimicrobial studies

Antimicrobial studies have been carried out using Agar Well diffusion method against the Gram positive bacteria assay namely *Staphylococcus aureus* and *Streptococcus pneumonia* and Gram negative bacteria *Klebsiella pneumonia*, *Pseudomonas aeruginosa*, and *Escherichia coli*. For antifungal screening, the disc diffusion method[48] was used against fungi *Candida albicans*, *Aspergillus flavus*, and *Aspergillus niger*. Gentamicin was used as a standard drug for antibacterial screening and amphotericin B for antifungal screening.

## 2.9 | DNA binding studies

DNA binding studies were performed using a spectrophotometric titration method. Experiments involving the interaction of compounds with CT-DNA were performed

using double distilled water with tris (hydroxymethyl) aminomethane (Tris, 5 mM) and sodium chloride (50 mM). The pH was adjusted, and the absorption titration experiments were performed by maintaining 50 μg/ml of the concentration of the title compound as constant but with variable CT-DNA concentration from 10 to 50 μM. While measuring the absorption spectra, equal amounts of DNA were added to both complex and reference solutions to eliminate the absorbance of DNA itself. The data were then fit into the following equation, and the intrinsic binding constant $K_b$ was calculated.

$$[\mathrm{DNA}]/(\varepsilon_a-\varepsilon_f) = [\mathrm{DNA}]/(\varepsilon_b-\varepsilon_f) + 1/[K_b(\varepsilon_b-\varepsilon_f)] \quad (1)$$

where [DNA] is the concentration of DNA in base pairs, $\varepsilon_a$ the apparent absorption coefficient, $\varepsilon_f$ the extinction coefficient of the free compound, and $\varepsilon_b$ the extinction coefficient of the compound when fully bound to DNA respectively. In the plots of [DNA]/ ($\varepsilon_a$-$\varepsilon_f$) vs [DNA], the ratio of a slope to the intercept gives the $K_b$ value.[49]

## 3 | RESULTS AND DISCUSSION

### 3.1 | Crystal structure analysis using SCXRD

Single crystals of the title compound were collected and subjected to SCXRD analysis. Crystallographic data and structure refinement details of **M3P** are shown in Table 1. Figure 1 shows ORTEP view and thermal ellipsoids. The single-crystal X-ray diffraction data show that it crystallizes in a space group of P-1. The crystal belongs to triclinic system with the following lattice parameters: a = 9.8224(12) Å, b = 11.6383(14) Å, c = 11.8865(14) Å, α = 64.6410(10)°, β = 81.156(2)°, and γ = 69.5910(10)°, and its unit cell volume is 1150.8(2) Å$^3$.

Crystal structural analysis of the compound revealed the presence of abundant non-covalent (weak bonding) interactions such as intermolecular H-bonds, π–π stacking, and Van der Waals forces. Figure 2(a) shows the unit cell packing arrangement of **M3P** viewed through a* axis. Intermolecular H-bonding (Figure 2(b)) was observed with the hydrogen atom in the mesityl ring in one **M3P** moiety as a donor with the oxygen atom in the 2-pyridone ring of another neighboring **M3P** moiety as an acceptor. The inter-planar distance and angle between pyridone (A) and pyridone (B) rings [1.021 Å, 120.6(2)°] made the formation of the zig-zag-type of arrangement. Intermolecular hydrogen bonds are also observed in the crystal packing which are formed between the hydrogen atom of the water molecule present in the crystal with the oxygen atom of the pyridone ring. The sp$^3$ C-H of mesityl moiety and pyridone ring of **M3P** is associated with the adjacent molecules to make two sp$^3$ C–H$^{\cdots}$π and two sp$^3$ C–H$^{\cdots}$ C interactions. These sp$^3$ C–H$^{\cdots}$ π and sp$^3$ C–H$^{\cdots}$ C interactions developed a typical edge-to-edge arrangements through mesityl moiety and pyridone ring with two neighboring **M3P** molecules. **M3P** exhibited π–π stacking interactions in the crystal due to their aromatic moieties with a short contact distance <3.7 Å. Three π–π stacking interactions were observed between mesityl moiety and pyridone ring of **M3P (A)** with **M3P (C).** These π–π stacking interactions created the perpendicular arrangement of mesityl moiety and pyridone ring in **M3P,** and these intermolecular interactions generated a slip stacking arrangement with neighboring molecules. The π$^{\cdots}$ π stacking modes formed in **M3P(A)** and **M3P (B)** namely C2(A)-C17(B) mesityl$^{\cdots}$ mesityl with a distance of 4.02 Å, C11(A)-C19(B) pyridone–pyridone with a distance of 3.75 Å and mesityl-pyridone C12(A)-C20 (B) with 3.58 Å displayed the existence of π–π stacking interactions in the crystal between the aromatic mesityl and pyridone moieties of **M3P (A)** and **M3P (B)** (Figure 2(c)). The stacking pairs are not completely parallel to each other. Hence, these π–π stacking interactions created face-to-face 3-D parallel-displaced arrangements throughout the crystal.[50] The **M3P** crystal packing forms a supramolecular sheet like arrangement (Figure 2 (d)) in which the water molecule in the lattice acts as a bridge between the layers.

The molecular structure of the compound is composed of three pyridone rings and one mesityl ring. In **M3P**, the torsion angles of C(2)-C(1)-C(10)-N(1), C(4)-C(3)-C(16)-N (2), C(6)-C(5)-C(22)-N(3) are 179.51(19), 97.90(2), and 102.00(2), respectively. The torsion angle 97.90(2) represents that one of the pyridone rings is perpendicular to the mesityl ring. The triclinic crystals of **M3P** showed the orientation of pyridone rings; that is, A N1 (C11-C15), B N2 (C17-C21), and C N3 (C23-C37) are perpendicular with respect to the central aromatic ring (C1-C6) having dihedral angels of 86.20°, 70.20°, and 77.00°, respectively.[51]

### 3.2 | Hirshfeld surface and 2D fingerprint plot analysis

The area and volume of three-dimensional Hirshfeld surface mapped on $d_{norm}$, di, de, curvedness and shape index properties are 566.43A$^2$ and 483.73A$^3$, respectively. The Hirshfeld surface of **M3P** mapped over a $d_{norm}$ is shown in Figure 3. The Hirshfeld surface mapped with $d_{norm}$ was generated with the color scale of −0.5016 (a.u) for red and 1.6293 (a.u) for blue. The bright red color spot inside the contour highlighted the intermolecular interactions in the crystal structure. The hydrogen bond contact between

**TABLE 1** Crystal data and structure refinement

| **CCDC number** | **1,495,831** | |
|---|---|---|
| Empirical formula | $C_{27}\ H_{29}\ N_3\ O_4$ | |
| Formula weight | 459.53 | |
| Temperature | 110.0 K | |
| Wavelength | 0.71073 Å | |
| Crystal system | Triclinic | |
| Space group | P-1 | |
| Unit cell dimensions | a = 9.8224(12) Å | α = 64.6410(10)° |
| | b = 11.6383(14) Å | β = 81.156(2)° |
| | c = 11.8865(14) Å | γ = 69.5910(10)° |
| Volume | 1150.8(2) $Å^3$ | |
| Z | 2 | |
| Density (calculated) | 1.326 $mg/m^3$ | |
| Absorption coefficient | 0.090 $mm^{-1}$ | |
| F(000) | 488 | |
| Crystal size | 0.259 × 0.156 × 0.058 $mm^3$ | |
| Theta range for data collection | 1.896 to 27.620°. | |
| Index ranges | -12 < =h < =12, -13 < =k < =15, 0 < =l < =15 | |
| Reflections collected | 9,538 | |
| Independent reflections | 9,538 | |
| Completeness to theta | 25.242° 100.0 % | |
| Absorption correction | Semi-empirical from equivalents | |
| Max. and min. transmission | 0.7456 and 0.6817 | |
| Refinement method | Full-matrix least squares on $F^2$ | |
| Data/restraints/parameters | 9538/0/314 | |
| Goodness-of-fit on $F^2$ | 1.035 | |
| Final *R* indices [I > 2sigma(I)] | R1 = 0.0558, wR2 = 0.1344 | |
| R indices (all data) | R1 = 0.0958, wR2 = 0.1561 | |
| Extinction coefficient | n/a | |
| Largest diff. peak and hole | 0.885 and −0.277 e.$Å^{-3}$ | |

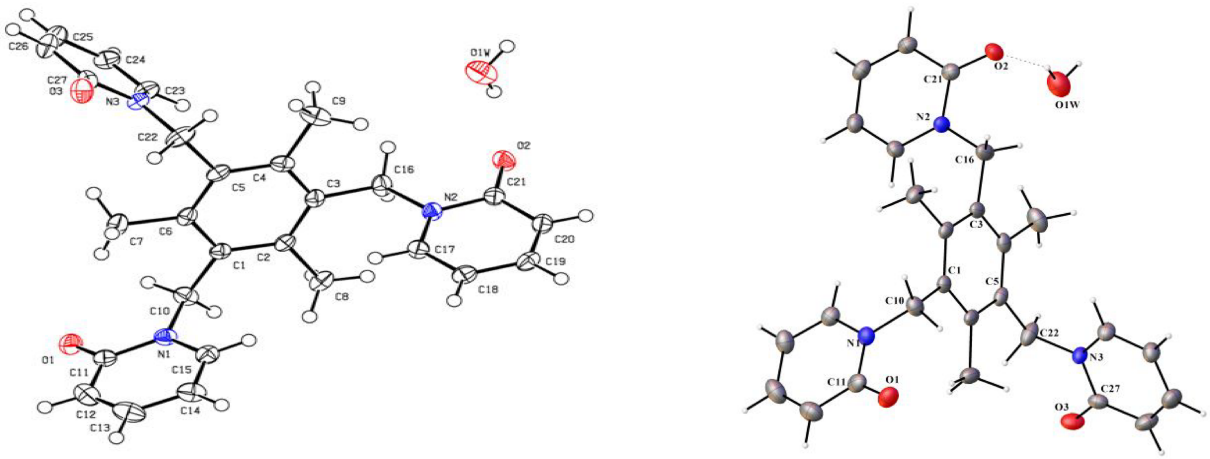


**FIGURE 1** An ORTEP view and thermal ellipsoid of M3P

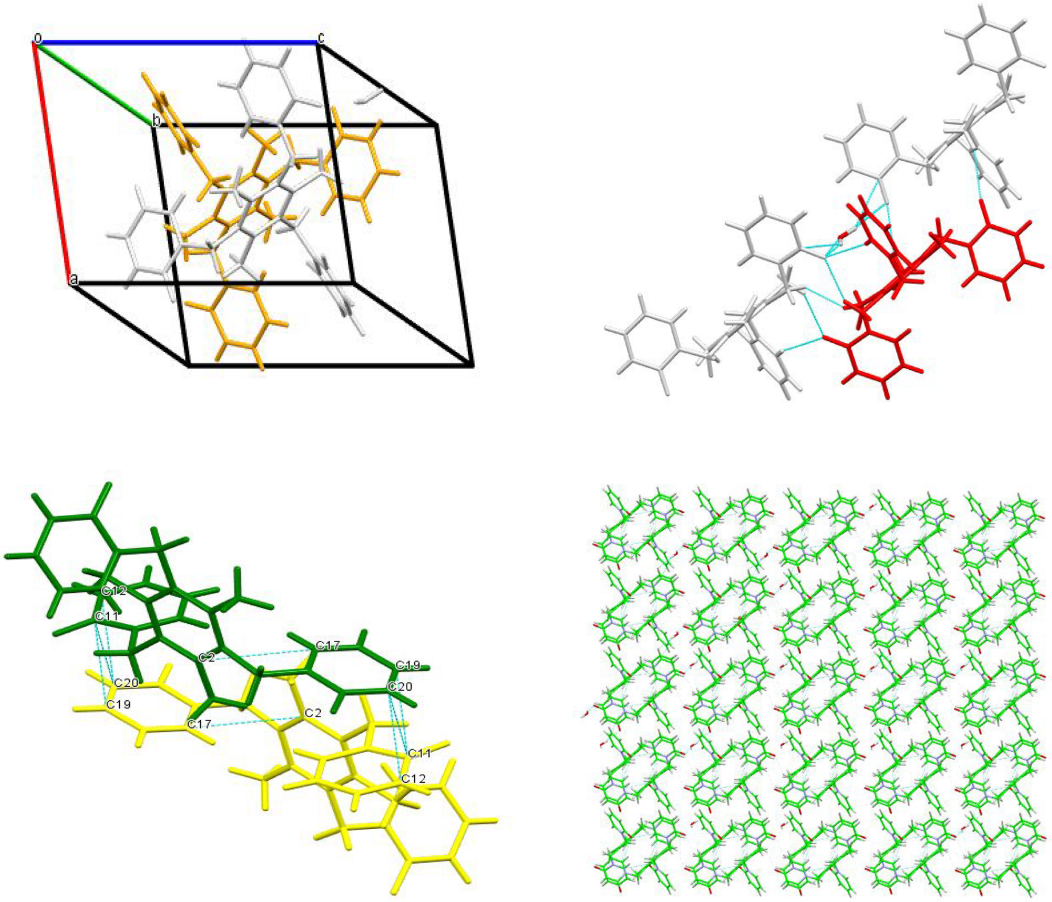


**FIGURE 2** (a) Unit cell packing arrangement viewed through crystallographic a*-axis, (b) hydrogen bonding, (c) stacking interactions, and (d) sheet-like arrangement viewed through crystallographic *b*-axis

hydrogen in water and carbonyl oxygen could be seen over the Hirshfeld surface as bright red spots. The red spots over the surface arise due to weak C-H···C-H and C-H···π interactions, where the intermolecular distance between neighboring molecules is less than Van der Waals radius. In the blue region on the Hirshfeld surface, the intermolecular distance between neighboring molecules is more than Van der Waals radius. The Hirshfeld surface of **M3P** mapped over shape index and curvedness is shown in Figure 3. Hirshfeld surface mapped over shape index is the most sensitive method to determine the changes in the surface shape of the molecule and can be used to identify the two molecular Hirshfeld surfaces which touch one another. The red triangles on them represented by hollow regions indicated atoms of the π-stacked molecule above them, and the blue triangles represented by bumps indicated the atoms of the molecule inside the surfaces. As it can be seen from Figure 3 the shape index plot has complementary red and blue spots which indicated the stacking of molecules related by center of symmetry. The curvedness mapped over Hirshfeld surface provided useful information about the shape of the surface of the molecule. Curvedness maps typically showed green flat areas of the surface that corresponds to low values of curvedness, separated by dark blue curvature areas which correspond to high values of curvedness and thus divide the surface into patches, indicating interactions between neighboring molecules.[52] The curvedness map of the compound as shown in Figure 3 showed the presence of green flat patches present over pyridine moiety indicating the planar π–π stacking between neighboring molecules. In di, the color scale in the conformations was maintained as 0.8022 (a.u) for red and 2.9108 (a.u) for blue. The fingerprint plot created by combining di and de described a 2D representation of 3D Hirshfeld surface and provides a summary of intermolecular contacts in the same way as the Hirshfeld surface. The fingerprint plots for different intermolecular interactions and Hirshfeld surfaces corresponding to these interactions are given in Figure 4. The summary of these contacts including reciprocal contacts and their contributions are shown in Table 2. It can be observed that the major interaction between neighboring molecules is between hydrogen atoms, that is, H···H which covers 56.3% of all interactions. The strong

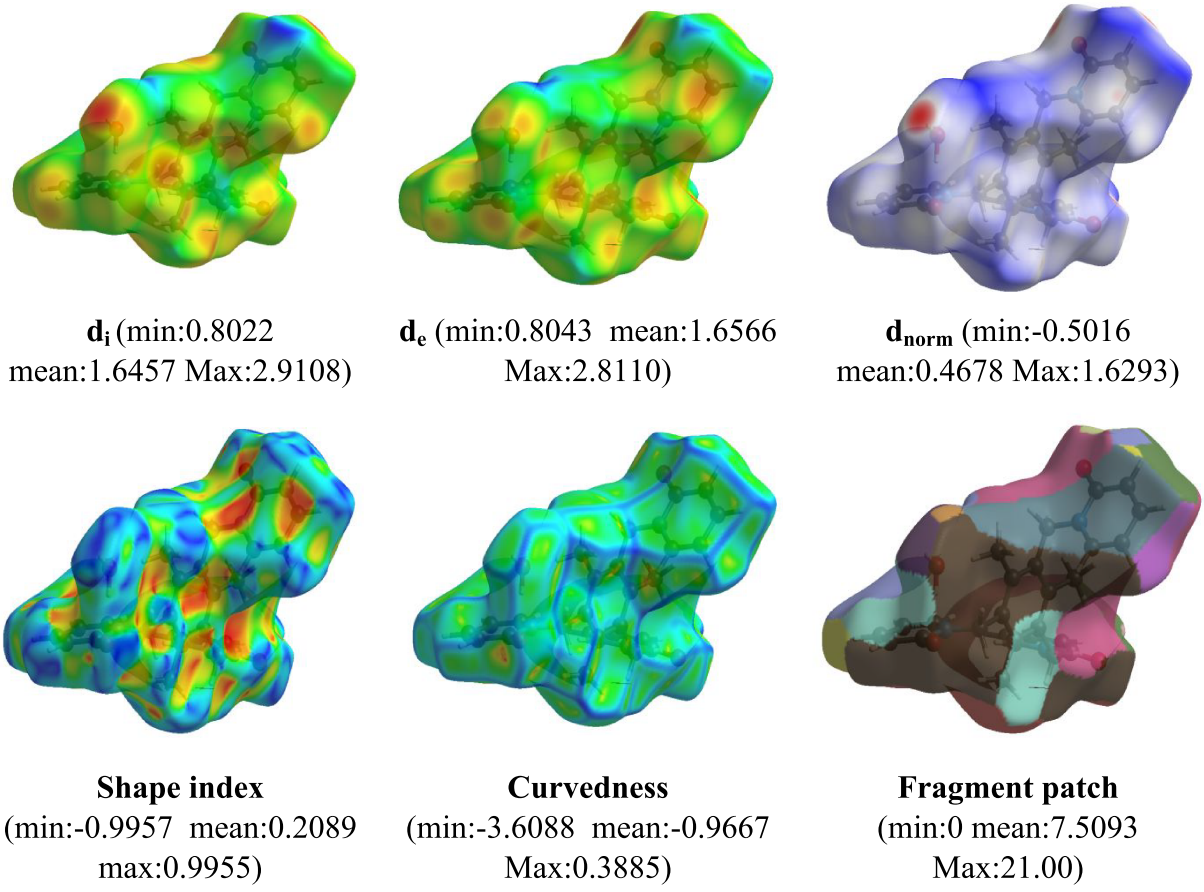


**FIGURE 3** Hirshfeld surface of M3P

hydrogen bond interactions between O···H/H···O are represented by two large spikes at the bottom of the fingerprint plot and accounted for 20.5% of all interactions. This interaction is also indicated by two bright red spots on the Hirshfeld surface (Figure 4). The fingerprint plots show that H-C/C-H contacts comprise 18% of the total Hirshfeld surface area for the molecule. They correspond to all O-H···O interactions of which strong C-H···π interactions appear as four light red spots on the Hirshfeld surface (Figure 4). The contact between Carbon and Carbon (C-C/C-C) is another interaction comprising 3.4% of all other interactions. This interaction is characterized by two small spikes on sides of the fingerprint plot as shown in Figure 4. The other minor contacts include C-N (0.7%), N-H (0.6%), and C-O (0.4%) which account for the remaining 7.3% of all interactions over Hirshfeld surface.

## Theoretical studies

The energies of compounds were calculated at the B3LYP/6-311G++ level of theory by the DFT method in the gas phase, carried out from the experimental structures.[53–57] Parameters like total energy, $E_{HOMO}$, $E_{LUMO}$, ionization potential, electron affinity, electronegativity, electrochemical potential, hardness, softness, and nucleophilicity are given in Table 3. According to Molecular Orbital (MO) theory, the Highest Occupied Molecular Orbital (HOMO) and the Lowest Unoccupied Molecular Orbital (LUMO) are collectively called frontier molecular orbitals (FMOs). FMOs are the most important factors affecting the bioactivity which specifies how the molecule interacts with species. The interaction between the molecule and the receptor of bacteria is dominated by π–π stacking and hydrophobic interaction among these FMOs.[58,59] HOMO and LUMO of compounds are demonstrated in Figure 5. The electron clouds in **M3P** showed that HOMO was located in one pyridone (ring-I) and the LUMO in another pyridone ring and not in the mesityl moiety. This confirmed the presence of intermolecular π–π stacking interactions between pyridone units. The energy of the HOMO is linked to the ionization potential, while LUMO energy is linked to the electron affinity. The results reveal that the energy of the HOMO orbital is equal to −5.7470 eV, and the energy of the LUMO orbital is equal to −1.2030 eV, which gives

an energy gap of about −4.5440 eV. This energy gap describes well the molecular chemical reactivity.[60,61] From Table 3, the parameters such as Ionization Potential (I), Electron Affinity (A), and Electronic Chemical Potential (μ) are equal to −5.7470, 1.2030, and −3.4750 eV, respectively. The chemical hardness (η) is found to be 2.2720 eV. Also, the molecule has a chemical softness equal to 0.4401 $eV^{-1}$. The electronegativity is computed based on the HOMO and LUMO energies and is found to be 3.4750 eV. The nucleophilicity value is found to be 3.6342. Finally, the maximum charge transfer index has been calculated and found to be 1.529. Mulliken atomic charge calculation plays a major role in the quantum chemical calculations of the molecular system. As the

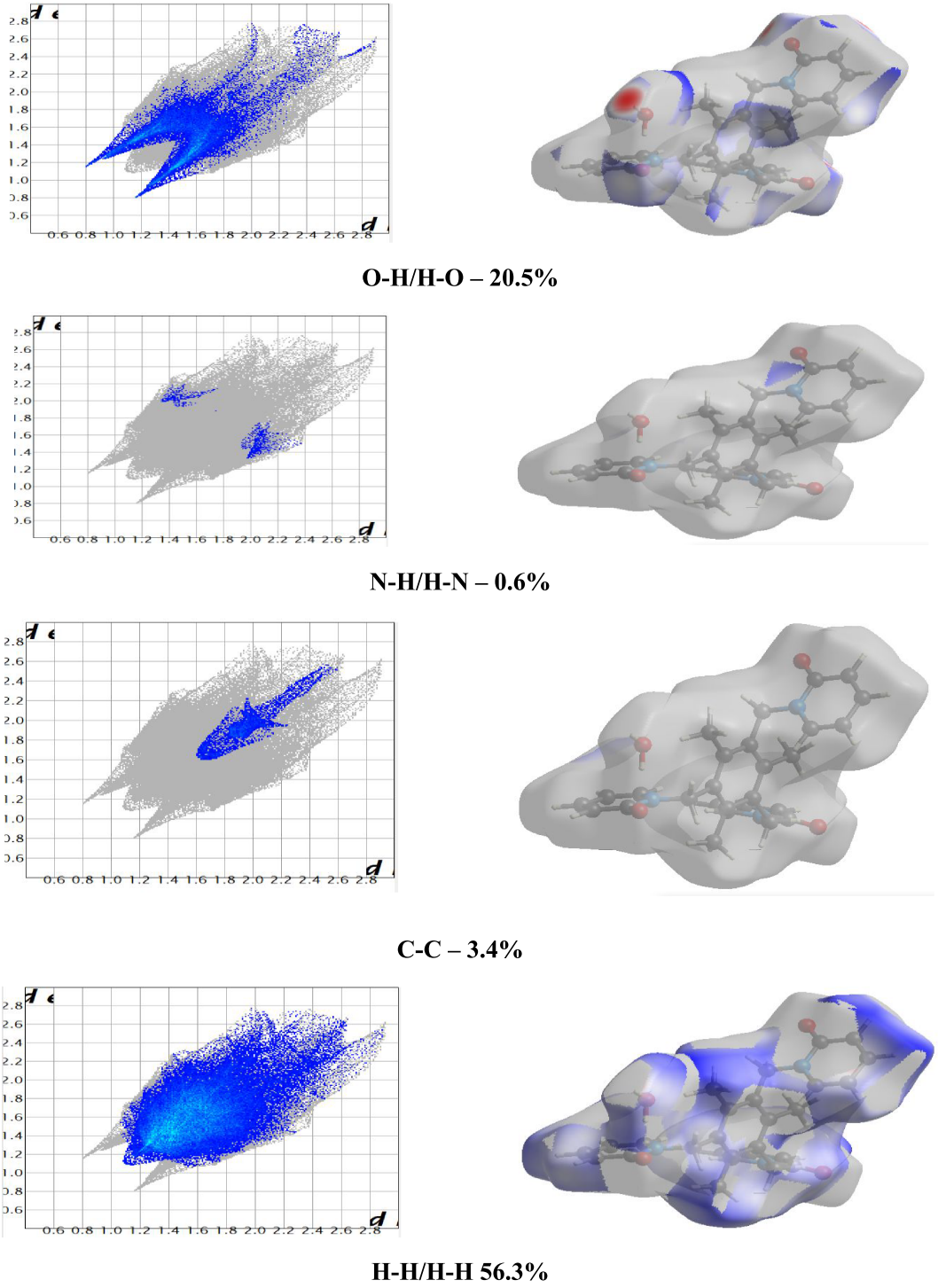


**FIGURE 4** Fingerprint plot with contribution of various interactions for M3P

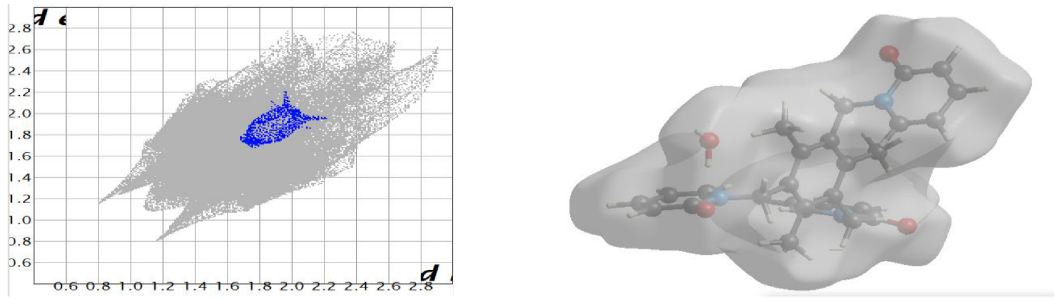

C-N/N-C – 0.7%

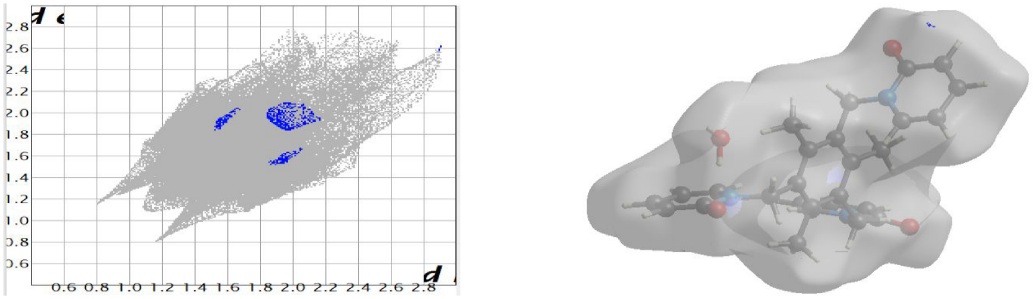

C-O/O-C – 0.4%

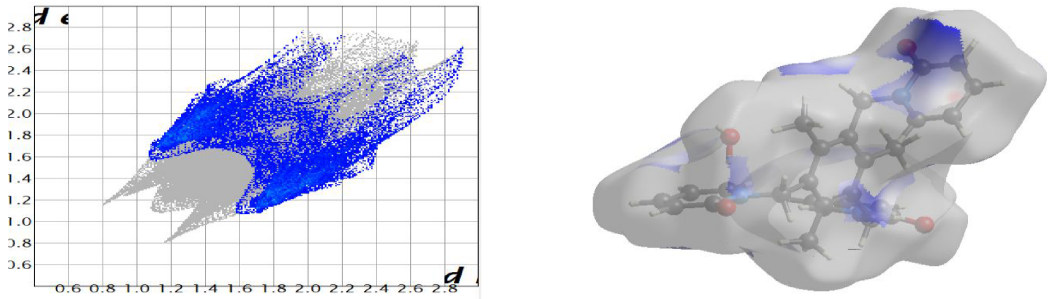

C-H/H-C – 18%

**FIGURE 4** (Continued)

system of electronic structure, dipole moment, polarizability, and other molecular properties is affected by atomic charges, the distribution of charge over the atoms leads to the creation of donor and acceptor pairs producing charge transfer in the molecule. The Mulliken population analysis in M3P molecule was computed using B3LYP with 6-311G++ (d,p) basis set and is listed in Table 4. In our molecule, the O61 atom has the highest negative charge (−0.616) compared to other oxygen atoms (O1 = −0.5796, O2 = −0.5939, and O3 = −0.5684) present in the rings. The carbon atom involved with the hydrogen atom is negative, whereas the remaining carbon atoms are positively charged in **M3P**. The oxygen and nitrogen atoms have more negative charge, whereas all the hydrogen atoms have positive charges. The more positive charge of carbon is found in the atoms C28, C40, C48, and C60. It is mainly due to the substitution of negative charge of oxygen and nitrogen atoms. The presence of a large negative charge on O2 and the net positive charge on H62, H63 atom may confirm the formation of C48-O27 ... H63 intermolecular hydrogen bond interaction in solid state.

## 3.3 | Molecular docking studies

Molecular docking techniques are used to recognize the drug–DNA interactions in rational drug design, as well as in the mechanistic study by placing a small molecule into the binding site of the target DNA.

The mode of interaction of the compound with DNA was theoretically calculated by molecular docking studies using DNA base pairs d $(CGCGAATTCGCG)_2$ dodecamer (PDB ID: 355D) using the Auto Dock tools. Minimum

**TABLE 2** Summary of contacts (reciprocal contact included) and their contributions to the Hirshfeld surface in M3P

| Types of contacts | Percentage contributions |
|---|---|
| H-H | 56.3 |
| O-H | 20.5 |
| C-H | 18.0 |
| C-C | 3.4 |
| C-N | 0.7 |
| N-H | 0.6 |
| C-O | 0.4 |

**TABLE 3** FMO energy parameters and global reactivity descriptors of M3P

| Molecular properties | M3P |
|---|---|
| Total energy (kcal/Mol) | −1511.549 |
| $E_{HOMO}$ (eV) | −5.7470 |
| $E_{LUMO}$ (eV) | −1.2030 |
| ΔE (eV) | −4.5440 |
| Ionization potential (eV) | 5.7470 |
| Electron affinity (eV) | 1.2030 |
| Electronegativity (eV) | 3.4750 |
| Electrochemical potential (eV) | −3.4750 |
| Absolute hardness (eV) | 2.2720 |
| Softness (eV) | 0.4401 |
| Nucleophilicity (eV) | 3.6342 |
| Dipole moment (Debye) | 5.4148 |

energy conformation was obtained from the docking of the compound with CT-DNA (Figure 6). Further, the resulting structures are stabilized by Van der Waals and hydrogen bond interactions with DNA. Some important binding between donor and acceptor atoms is also available in the interactions. It reveals that the hydrogen and carbonyl oxygen atoms play an important role as donor atoms in hydrogen bonding. The binding energy of M3P is found to be −6.4 kcal/mol.

The action of the drug needs a comprehensive understanding of compounds–protein interactions which has a great role in rational drug designing.[62–65] Molecular docking results revealed that the binding affinity of M3P into the binding pocket of BSA protein is −8.1 kcal/mol. The most favorable docking poses are given in Figure 7. The hydrogen bonding interaction was observed between Asn404 with the oxygen atom of the pyridine ring. An interaction between Met547 and nitrogen atom of the M3P compound was also observed. The π–π interaction was also between Leu397 amino acid with the mesityl ring. Three amino acids namely Val408, Leu543, and Lys544 are involved in hydrophobic interactions with the compound.

## 3.4 | Antimicrobial evaluation

The M3P crystal was screened against some microorganisms to evaluate their antimicrobial activities. The crystal was evaluated for their in vitro antibacterial activity against some Gram positive bacteria assay namely *Staphylococcus aureus* and *Streptococcus pneumonia* and Gram negative bacteria *Klebsiella pneumonia*, *Pseudomonas aeruginosa*, and *Escherichia coli*. They were also evaluated for *their in vitro* antifungal potency against *Candida albicans*, *Aspergillus flavus*, and *Aspergillus niger* fungal strains. The agar-diffusion method was used in the determination of the preliminary antibacterial and antifungal activity. Gentamicin and amphotericin B were used as reference drugs for antibacterial and antifungal species respectively. The results were recorded for each

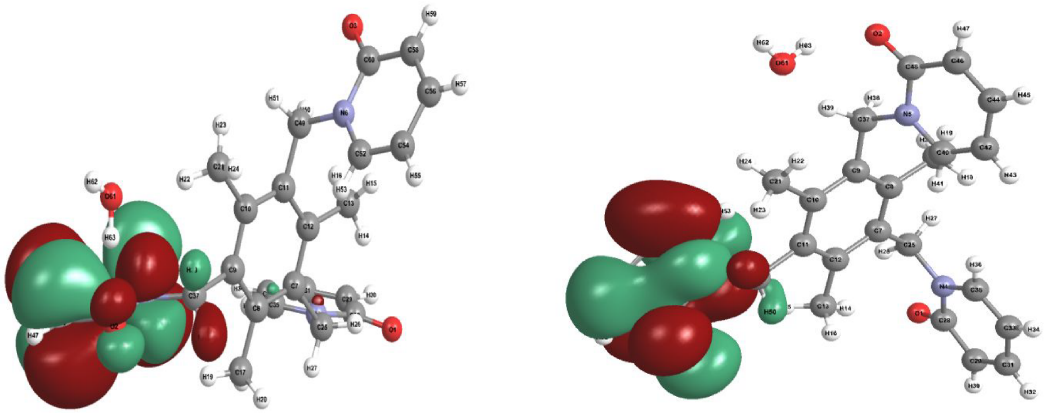

LUMO HOMO

**FIGURE 5** Molecular orbitals of M3P

**TABLE 4** Mulliken atomic charges of M3P

| Atoms | Charges | Atoms | Charges |
|---|---|---|---|
| O1 | −0.5796 | C33 | −0.1266 |
| O2 | −0.5939 | H34 | 0.0652 |
| O3 | −0.5684 | C35 | 0.1943 |
| N4 | −0.5099 | H36 | 0.0990 |
| N5 | −0.5285 | C37 | −0.0509 |
| N6 | −0.5310 | H38 | 0.1379 |
| C7 | −0.0319 | H39 | 0.1495 |
| C8 | 0.0371 | C40 | 0.1985 |
| C9 | −0.0744 | H41 | 0.1084 |
| C10 | 0.0362 | C42 | −0.1294 |
| C11 | −0.0764 | H43 | 0.0660 |
| C12 | 0.0460 | C44 | 0.0006 |
| C13 | −0.3543 | H45 | 0.0760 |
| H14 | 0.1288 | C46 | −0.1215 |
| H15 | 0.1378 | H47 | 0.0753 |
| H16 | 0.1409 | C48 | 0.6078 |
| C17 | −0.3576 | C49 | −0.0273 |
| H18 | 0.1225 | H50 | 0.1468 |
| H19 | 0.1213 | H51 | 0.1255 |
| H20 | 0.1432 | C52 | 0.1901 |
| C21 | −0.3528 | H53 | 0.1057 |
| H22 | 0.1516 | C54 | −0.1251 |
| H23 | 0.1189 | H55 | 0.0659 |
| H24 | 0.1426 | C56 | −0.0056 |
| C25 | −0.0855 | H57 | 0.0728 |
| H26 | 0.1647 | C58 | −0.1242 |
| H27 | 0.1222 | H59 | 0.0749 |
| C28 | 0.5952 | C60 | 0.5856 |
| C29 | −0.1219 | O61 | −0.6160 |
| H30 | 0.0787 | H62 | 0.2879 |
| C31 | −0.0080 | H63 | 0.3032 |
| H32 | 0.0759 | | |

compound as the average diameter of inhibition zones (IZ) of bacterial or fungal growth around the discs in mm (Table 5).

The results revealed that most of the tested compounds displayed variable inhibitory effects on the growth of the tested bacterial strains and also against antifungal strains. From Table 5, it is clear that the antimicrobial activity depends upon the concentration of the compound used and a minimum inhibitory concentration of 100 μg/ml and above is needed to kill the microorganisms. It is noteworthy that M3P shows a good response

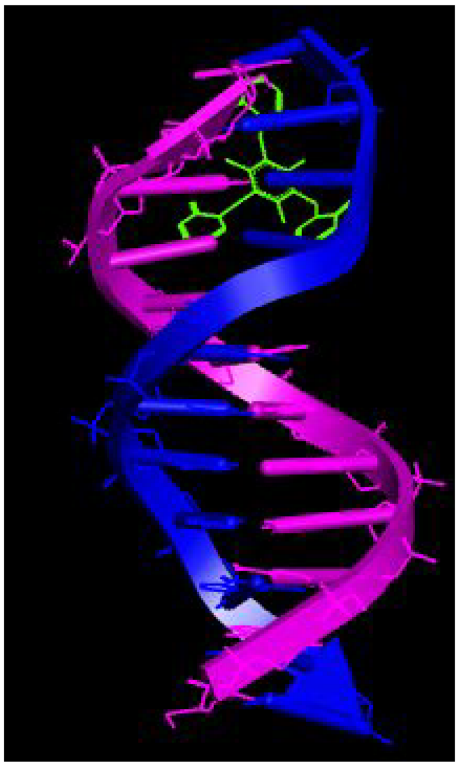

**FIGURE 6** Molecular docking studies of M3P with DNA

against *Pseudomonas aeruginosa* and *Klebsiella pneumonia* when compared with the standard drug gentamicin at a high concentration of 500 μg/ml. It shows moderate activity against *Staphylococcus aureus*, *Escherichia coli* and *Streptococcus pneumonia*. Antifungal screening of M3P exhibited moderate activity against *Aspergillus flavus* when compared with the standard drug amphotericin B. Further, M3P shows good activity against *Candida albicans* and *Aspergillus niger*. As evident from Table 5, inhibition against bacteria and fungi increases with an increase in the concentration of the compound.

## 3.5 | DNA binding studies using the spectrophotometric titration method

Electronic absorption spectroscopy is an effective method to determine the binding mode and intensity of organic molecules with CT-DNA. The intrinsic binding constant $K_b$ for **M3P** was calculated as $9.18 \times 10^4$ $M^{-1}$ indicating that it can moderately bind with CT-DNA which is comparable with the docking studies. There was another typical observation from the UV absorption spectrum that there was an increase in absorption for the compound while increasing the DNA concentration, that is, hyperchromic shifts have been observed for the compounds

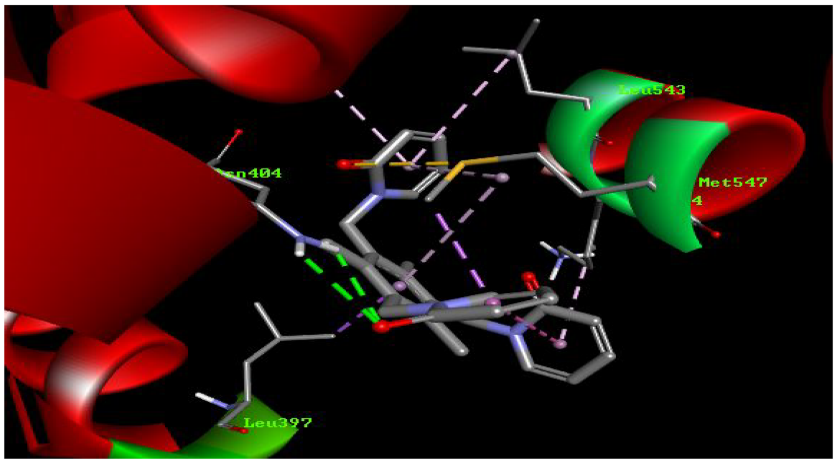


**FIGURE 7** Molecular docking of M3P with BSA

**TABLE 5** Antibacterial activity and antifungal activity of M3P

| | | Zone of inhibition (mm) | | | | |
|---|---|---|---|---|---|---|
| **No** | **Name of the bacteria and fungi** | **500 µg/ml** | **250 µg/ml** | **100 µg/ml** | **50 µg/ml** | **Std** |
| 1 | *Staphylococcus aureus (bacteria)* | 07–10 | 05–08 | 02–05 | 00–02 | 12–15 |
| 2 | *Streptococcus pneumonia (bacteria)* | 19–21 | 21–24 | 18–21 | 05–11 | 20–23 |
| 3 | *Klebsiella pneumonia (bacteria)* | **11–14** | 06–09 | 04–07 | 03–05 | 10–13 |
| 4 | *Pseudomonas aeruginosa (bacteria)* | **24–28** | 20–23 | 17–20 | 10–12 | 23–26 |
| 5 | *Escherichia coli (bacteria)* | 05–08 | 02–05 | 01–03 | 02–03 | 08–12 |
| 6 | *Candida albicans (fungi)* | **24–27** | 19–23 | 16–19 | 07–12 | 21–24 |
| 7 | *Aspergillus flavus (fungi)* | 08–11 | 05–08 | 06–09 | 04–07 | 12–15 |
| 8 | *Aspergillus Niger (fungi)* | **12–15** | 08–11 | 07–10 | 03–06 | 11–14 |

*Note*. The bold emphasis denotes the highest activity of the title compound against the bacteria and fungi.

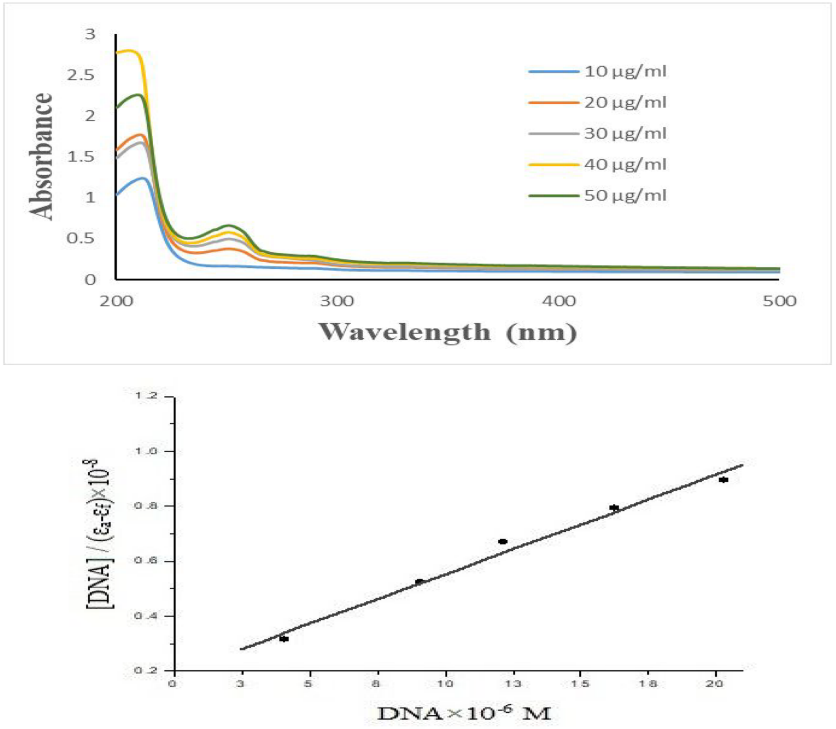


**FIGURE 8** UV-Vis spectra for DNA binding ability of M3P

(Figure 8). The absorption spectrum showed one significant peak at 255 nm (hyperchromism red shift). This hyperchromic effect is observed when the interactions of the chromophore (compound) with DNA are electrostatic or partially intercalative. This can result in the decoiling of DNA helix and thereby losing their H-bonds with the neighbor strand. Therefore, this decoiled DNA single-strand might absorb the ultraviolet light due to the presence of electrostatic atoms which result in hyperchromocity.[66]

## 4 | CONCLUSION

To sum up, a new crystal,1-({2,4,6-trimethyl-3,5-bis[(2-oxo-2H-pyridin-1-yl)methyl]phenyl}methyl)-2H-pyridin-2-one hydrate (M3P) has been synthesized and characterized by FT-IR, 1H-, and 13C-NMR and confirmed using single-crystal X-ray diffraction analysis. Crystal structural analysis of the compound revealed the slip stacking arrangement of molecules. Based on the structure analysis, the theoretical results (DFT) are in agreement with the experimental ones. Molecular interactions of the compound were investigated via Hirshfeld surface analysis. The DNA binding properties of the compound were examined by molecular docking studies as well as by UV spectroscopic method. The studies proved the binding efficiency of the compound with DNA. Antimicrobial evaluation showed good activity against bacteria (*Pseudomonas aeruginosa* and *Klebsiella pneumonia)* and fungi (*Candida albicans* and *Aspergillus niger).*

## ORCID

*R. Nandini Asha* https://orcid.org/0000-0002-8296-6380
*B. Ravindran Durai Nayagam* https://orcid.org/0000-0001-7859-971X

## REFERENCES

[1] A. Al-Mulla, *Der Pharma Chemica* **2017**, *9*, 141.
[2] M. Torres, S. Gil, M. Parra, *Org Chem* **2005**, *9*, 1757.
[3] J. Kohno, N. Hirano, K. Sugawara, M. Nishio, T. Hashiyama, N. Nakanishi, S. Komatsubara, *Tetrahedron* **2001**, *57*, 1731.
[4] Y. Fujita, H. Oguri, H. Oikawa, *Tetrahedron Lett.* **2005**, *46*, 5885.
[5] A. Fassihi, D. Abedi, L. Saghaie, R. Sabet, H. Fazeli, G. Bostaki, O. Deilami, H. Sadinpou, *Eur. J. Med. Chem.* **2009**, *44*, 2145.
[6] G. Semple, B. M. Andersson, V. Chhajlani, J. Georgsson, M. J. Johansson, Å. Rosenquist, L. Swanson, *Bioorg. Med. Chem. Lett.* **2003**, *13*, 1141.
[7] R. L. T. Parreira, O. Abrahão Jr., S. E. Galembeck, *Tetrahedron* **2001**, *57*, 3243.
[8] B. Dojer, A. Pevec, Z. Jaglicic, M. Krist, *J. Mol. Struct.* **2017**, *1128*, 724.
[9] R. Sheng, L. Tang, L. Jiang, L. Hong, Y. Shi, N. Zhou, Y. Hu, *ACS Chem. Nerosci.* **2016**, *7*, 69.
[10] W. A. Loughlin, J. D. A. Tyndall, M. P. Glenn & D. P Fairlie. *Chem. Rev.*. **2004**, *104*, 6085.
[11] L. Costantino, D. Barlocco, *Curr. Med. Chem.* **2006**, *13*, 65.
[12] N. A. Hamdy, A. M. Gamal-Eldeen, *Eur. J. Med. Chem.* **2009**, *44*, 4547.
[13] G. Yu, P. P. Rao, M. A. Chowdhury, K. R. Abdellatif, Y. Dong, D. Das, C. A. Velázquez, M. R. Suresh, E. E. Knaus, *Bioorg. Med. Chem. Lett.* **2010**, *20*, 2168.
[14] S. K. Rai, P. Singh, S. Khanam, A. K. Tewari, *New J. Chem.* **2016**, *40*, 5577.
[15] M. Endoh, M. Hori, *Expert Opin. Pharmacother.* **2006**, *7*, 2179.
[16] E. Lo Presti, R. Boggia, A. Feltrin, G. Menozzi, P. Dorigo, L. Mosti, *Farmacoterapia* **1999**, *54*, 465.
[17] N. Mohammad Asif, *Am J. Med. Sci.* **2012**, *4*, 499.
[18] M. Urban, R. Pohl, B. Klepetarova, M. Hocek, *J. Org. Chem.* **2006**, *71*, 7322.
[19] D. Tauraite, R. Razanas, A. Mikalkenas, S. Serva, R. Meskys, *Nucleos Nucleot Nucl* **2016**, *35*, 163.
[20] A. Rudra, D. Hou, Y. Zhang, J. Coulter, H. Zhou, T. L. DeWeese, M. M. Greenberg, *J. Org. Chem.* **2015**, *80*, 10675.
[21] D. Ž. Mijin, J. M. Marković, D. V. Brković, A. D. Marinković, *Hem Ind* **2014**, *68*, 1.
[22] Q. Li, L. A. Mitscher, L. L. Shen, *Med. Res. Rev.* **2000**, *20*, 231.
[23] Y. Fu, D. Zhang, S.-Q. Zhang, Y.-X. Liu, Y.-Y. Guo, M.-X. Wang, S. Gao, L.-X. Zhao, F. Ye, *J. Agric. Food Chem.* **2019**, *67*, 11839.
[24] F. Ying, S.-Q. Zhang, Y.-X. Liu, J.-Y. Wang, S. Gao, L.-X. Zhao, F. Ye, *Ind. Crop Prod.* **2019**, *137*, 566.
[25] C. D. Nisheeth, K. M. Rajpara, V. V. Joshi, *Bioorg. Med. Chem. Lett.* **2013**, *23*, 2714.
[26] T. Mandal, S. Pathak, A. Dey, M. M. Islam, S. K. Seth, A. A. Masum, J. Ortega-Castro, P. P. Ray, A. Frontera, S. Mukhopadhyay, *ACS Omega* **2019**, *4*, 7200.
[27] A. D. Becke, *JChem Phys* **2014**, 140.
[28] T. R. Julian, L. J. William, *J Chem Theory Comput* **2008**, *4*, 2297.
[29] A. W. van der Made, R. H. van der Made, *J. Org. Chem.* **1993**, *58*, 1262.
[30] APEX3 BRUKER AXS Inc., 5465 East Cheryl Parkway, Madison, USA WI 53711-5373.
[31] SADABS, BRUKER AXS Inc., 5465 East Cheryl Parkway, Madison, WI 53711-5373 USA.
[32] G. M. Sheldrick, *ActaCryst* **2008**, *A64*, 112.
[33] G. M. Sheldrick, *ActaCryst* **2015**, *A71*, 3.
[34] G. M. Sheldrick, *ActaCryst* **2015**, *C71*, 3.
[35] XT, XS, BRUKER AXS Inc., 5465 East Cheryl Parkway, Madison, WI 53711-5373 USA.
[36] O. V. Dolomanov, L. J. Bourhis, R. J. Gildea, J. A. K. Howard, H. Puschmann, *J. Appl. Cryst.* **2009**, *42*, 339.
[37] J. J. McKinnon, D. Jayatilaka, M. A. Spackman, *Chem. Commun.* **2007**, *37*, 3814.
[38] M. A. Spackman, J. J. McKinnon, *CrstEngComm* **2002**, *4*, 378.
[39] C. F. Mackenzie, P. R. Spackman, D. Jayatilaka, M. A. Spackman, *IUCrJ* **2017**, *4*, 575.
[40] M. W. Schmidt, K. K. Baldridge, J. A. Boatz, S. T. Elbert, M. S. Gordon, J. H. Jensen, S. Koseki, N. Matsunaga, K. A. Nguyen, S. Su, T. L. Windus, M. Dupuis, J. A. Montgomery, *J. Comput. Chem.* **1993**, *14*, 1347.

[41] G. S. Suresh Kumar, A. Antony MuthuPrabhu, N. Bhuvanesh, *J. Mol. Struct.* **2014**, *1075*, 166.
[42] A. A. M. Prabhu, V. K. Subramanian, N. Rajendiran, *Spectrochim. Acta a Mol. Biomol. Spectrosc.* **2012**, *96*, 95.
[43] T. Sivasankar, A. A. M. Prabhu, M. Karthick, N. Rajendiran, *J Mol Stuct* **2012**, *1028*, 57.
[44] O. Trott, A. J. Olson, *J. Comput. Chem.* **2010**, *31*, 455.
[45] A. Bujacz, *Acta Crystallogr. D Biol. Crystallogr.* **2012**, *68*, 1278.
[46] R. Herowatia, G. P. Widodo, *Procedia Chem* **2014**, *13*, 63.
[47] M. Jahanshahtalab, M. Kamshad, S. Rezaei, S. Beigoli, A. S. Rad, J. Mehrzad, S. K. Moghadam, P. Mokaberi, S. Gharebaghi, M. R. Saberi, J. Chamani, J. Iran, *Chem Soc* **2019**, *16*, 1311.
[48] A. Alastruey-Izquierdo, M. S. Melhem, L. X. Bonfietti, J. L. Rodriguez-Tudela, *Rev. Inst. Med. Trop. Sao Paulo* **2015**, *57*, 57.
[49] C. Daisy, R. Nandini Asha, G. S. Suresh Kumar, E. Vadivel, N. Bhuvanesh, B. R. D. Nayagam, *J. Mol. Struct.* **2020**, *1222*, 128894.
[50] Z. F. Yao, J. Y. Wang, J. Pei, *Cryst. Growth des.* **2018**, *18*, 7.
[51] M. S. Al-Said, M. M. Ghorab, H. A. Ghabbour, S. Arshadc, H.-K. Fun, *ActaCryst* **2012**, *E68*, o1679.
[52] M. A. Spackman, D. Jayatilaka, *CrstEngComm* **2009**, *11*, 19.
[53] A. D. Becke, *J Chem Phys* **2014**, *140*, 1.
[54] T. R. Julian, L. J. William, *J Chem Theory Comput* **2008**, *4*, 297.
[55] P. J. Stephens, F. J. Devlin, C. F. Chabalowski, M. J. Frisch, *J. Phys. Chem.* **1994**, *98*, 11623.
[56] B. G. Johnson, P. M. W. Gill, J. A. Pople, *J. Chem. Phys.* **1993**, *98*, 5612.
[57] A. D. Becke, *J. Chem. Phys.* **1993**, *98*, 5642.
[58] S. Gatfaoui, I. Noureddine, T. Roisnel, H. Marouani, *J. Mol. Struct.* **2019**, *1191*, 183.
[59] R. E. Stratmann, G. E. Scuseria, M. J. Frisch, *J. Chem. Phys.* **1998**, *109*, 8218.
[60] N. Issaoui, H. Ghalla, S. A. Brandán, F. Bardak, H. T. Flakus, A. Atac, B. Oujia, *J. Mol. Struct.* **2017**, *1135*, 209.
[61] A. Rauk, **2001**, second ed., Wiley Interscience, New York.
[62] J. Lakshmipraba, S. Arunachalam, R. V. Solomon, P. Venuvanalingam, A. Riyasdeen, R. Dhivya, M. A. Akbarsha, *J. Biomol. Struct. Dyn.* **2015**, *33*, 877.
[63] J. Lakshmipraba, S. Arunachalam, R. Vijay Solomon, P. Venuvanalingam, *J Coord Chem* **2015**, *68*, 1374.
[64] D. Mustard, D. W. Ritchie, *Bioinformatics* **2005**, *60*, 269.
[65] R. Rohs, I. Bloch, H. Sklenar, Z. Shakked, *Nucleic Acids Res.* **2005**, *33*, 7048.
[66] B. Barare, M. Yildiz, H. Unver, K. Aslan, *TetrahedronLett* **2016**, *57*, 537.

## SUPPORTING INFORMATION

Additional supporting information may be found online in the Supporting Information section at the end of this article.

**How to cite this article:** Asha RN, Rahini MU, Daisy C, Nayagam BRD, Bhuvanesh N. Experimental and theoretical studies of 1,3,5-tris (bromomethyl)-2,4,6-trimethylbenzene with 2-pyridone. *J Phys Org Chem*. 2021;34:e4188. https://doi.org/10.1002/poc.4188